Cytoarchitectureal changes in hippocampal subregions of the NZB/W F1 mouse model of lupus

Graïc J-M.[1], Finos L.[2], Vadori V [5], Cozzi B.[1], Luisetto R.[3], Gerussi T.[1], Gatto M. [4], Doria A.[4], Grisan E[5]., Corain L.[2], Peruffo A.[1]

[1]Department of Comparative Biomedicine and Food Science, University of Padova, (35020), Italy

[2]Department of Statistical Sciences, University of Padova, Padova, (35100), Italy

[3]Department of Surgery, Oncology and Gastroenterology, University of Padova, Padova, (35100), Italy

[4]Rheumatology Unit, Department of Medicine (DIMED), University of Padova, Padova, (35100), Italy

[5]School of Engineering, London South Bank University, London, SE1 0AA, UK

[6]Department of Management and Engineering, University of Padova, Vicenza, (36100), Italy

Corresponding Author

Dr. Antonella Peruffo

Department of Comparative Biomedicine and Food Science

University of Padova

viale dell'Università 16, 35020 Legnaro (PD) – ITALY

phone +39.049.8272637

mail *antonella.peruffo@unipd.it*

Running title: Hippocampal neurons hypertrophy in NZB/W F1 mouse

Number of pages: 30

Number of figures (7), tables (3)

Number of words for abstract (246), introduction (548), and discussion (1522)

Conflict of interest statement: The authors declare that they have no conflict of interests.

Funding – Acknowledgments: This study was supported by a University of Padova Grant (BIRD # 179299/17) to Antonella Peruffo.

Keywords: Neurolupus, NZB/NZW F1, lupus model, Hippocampus, Cytoarchitecture, Multivariate analysis.

Cytoarchitectureal changes in hippocampal subregions of the NZB/W F1 mouse model of lupus

Graïc J-M.[1], Finos L.[2], Vadori V.[5,] Cozzi B.[1], Luisetto R.[3], Gerussi T.[1], Gatto M. [4], Doria A.[4], Grisan E[5]., Corain L.[2], Peruffo A.[1]

[1]Department of Comparative Biomedicine and Food Science, University of Padova, (35020), Italy

Department of Statistical Sciences, University of Padova, Padova, (35100), Italy

[3]Department of Surgery, Oncology and Gastroenterology, University of Padova, Padova, (35100), Italy

[4]Rheumatology Unit, Department of Medicine (DIMED), University of Padova, Padova, (35100), Italy

[5]School of Engineering, London South Bank University, London, SE1 0AA, UK

[6]Department of Management and Engineering, University of Padova, Vicenza, (36100), Italy

Corresponding Author

Dr. Antonella Peruffo

Department of Comparative Biomedicine and Food Science

University of Padova

viale dell'Università 16, 35020 Legnaro (PD) – ITALY

phone +39.049.8272637

mail *antonella.peruffo@unipd.it*

Running title: Hippocampal neurons hypertrophy in NZB/W F1 mouse

Number of pages: 30

Number of figures (7), tables (3)

Number of words for abstract (246), introduction (548), and discussion (1522)

Conflict of interest statement: The authors declare that they have no conflict of interests.

Funding – Acknowledgments: This study was supported by a University of Padova Grant (BIRD # 179299/17) to Antonella Peruffo.

Keywords.

Neurolupus, NZB/NZW F1, lupus model, Hippocampus, Cytoarchitecture, Multivariate analysis.

Abstract

Over 50% of clinical patients affected by the systemic lupus erythematosus disease display impaired neurological cognitive functions and psychiatric disorders, a form called neuropsychiatric systemic lupus erythematosus. Hippocampus is one of the brain structures most sensitive to the cognitive deficits and psychiatric disorders related to neuropsychiatric lupus. The purpose of this study was to compare, layer by layer, neuron morphology in lupus mice model NZB/W F1 *versus* Wild Type mice. By a morphometric of cells identified on Nissl-stained sections, we evaluated structural alterations between NZB/W F1 and Wild Type mice in seven hippocampal subregions: Molecular dentate gyrus, Granular dentate gyrus, Polymorph dentate gyrus, Oriens layer, Pyramidal layer, Radiatum layer and Lacunosum molecular layer. By principal component analysis we distinguished healthy Wild Type from NZB/W F1 mice. In NZB/W F1 mice hippocampal cytoarchitecture, the neuronal cells resulted larger in size and more regular than those of Wild Type. In NZB/W F1, neurons were usually denser than in WT. The Pyramidal layer neurons were much denser in Wild Type than in NZB/W F1. Application of principal component analysis, allowed to distinguish NZB/W F1 lupus mice from healthy, showing as NZBW subjects presented a scattered distribution and intrasubject variability. Our results show a hypertrophy of the NZB/W F1 hippocampal neurons associated with an increase in perikaryal size within the CA1, CA2, CA3 region and the DG. These results help advance our understanding on hippocampal organization and structure in the NZB/W F1 lupus model, suggesting the hypothesis that the different subregions could be differentially affected in neuropsychiatric systemic lupus erythematosus disease. Leveraging an in-depth analysis of the morphology of neural

cells in the hippocampal subregions and applying dimensionality reduction using PCA, we propose an efficient methodology to distinguish pathological NZBW mice from WT mice."

1. Introduction

Systemic Lupus Erythematosus (SLE) is an auto-immune disease that affects a variety of organ systems by altering the regulatory pathways of inflammation (Ghirardello et al. 2004), including the central nervous system (CNS) (Leung et al, 2016). Up to 75% of SLE patients show neurological symptoms involving a range of cognitive deficits, psychiatric disorders (Briani et al., 2009) and memory loss. This form is termed neuropsychiatric SLE (NPSLE). Beyond the existence of these symptoms, the full spectrum of NPSLE manifestation remains poorly understood (Schwartz et al, 2019). One of the brain regions most suspected to have marked NPSLE-related changes is the hippocampus. Critically involved in fundamental processes such as learning, emotions, spatial navigation and memory, the hippocampus is among the most studied neural systems in mammals. The *hippocampus proper* comprises the dentate gyrus (DG), CA1, CA2 and CA3 regions, each with their own cellular structure and distinctive functions. The three layers of the DG are the molecular layer (MoDG), granule cell layer (GrDG) and polymorph dentate gyrus (PoDG). Within the CA1, CA2 and CA3 regions, a number of layers are defined. The pyramidal layer (Py), the subregion in which the main cell types are pyramidal neurons, differing in terms of genetics, morphology, and connectivity (Merino-Serra et al., 2020). Deep to the Py is the *stratum oriens* (Or), a relatively cell-free subregion containing mostly fibers and some interneurons. Superficial to the Py is the *stratum radiatum* (Rad) and *stratum lacunosum-moleculare* (LMol) containing GABAergic interneurons, which play a critical role in modulating the dynamic activity in hippocampus networks (Jarsky et al., 2005).

Anatomical observations and lesioning experiments support the idea that the hippocampus is crucial in memory formation, especially the dentate gyrus (DG) area, while the CA3 area covers the encoding, storage and retrieval of memory (Hainmueller and Bartos, 2020). The hippocampus also

plays a major role in the formation of declarative, spatial, and contextual memory, as well as in the processing of emotional information and stress response (Zaletel et al., 2016).

The widely used NZB/W F1 (NZBW) murine model offers an opportunity to bridge the gap between neurological deficits and histological lesions underlying NPSLE (Pikman et al., 2017). NZBW mice spontaneously develop generalized auto-immune inflammation providing a powerful translational model to approach human autoimmune disease.

The neuronal loss and reduced neuronal density found in NZBW hippocampi were comparable to those described in human NPSLE patients (Ballok et al., 2004). The same year, Kowal and colleagues (Kowal et al., 2004) demonstrated that systemic immune responses could cause cognitive impairment even in the absence of an inflammatory cascade and suggested that the antibodies gained access to the brain to bind preferentially to hippocampal neurons, causing neuronal death with resulting cognitive dysfunction and altered hippocampal metabolism. More recent works focused on cellular and network basis of cognitive processes, allowing further understanding of the hippocampus role in complex memories processes (Lisman et al, 2017).

By advance quantitative imaging and statistical methods, over a large number of cells, we would like to contribute to the debate with hard evidence. In order to study quantitatively the fine changes in neuronal changes, and to quantify structural differences in the cytoarchitecture of NZBW and WT mice we set up an automatic pipeline combining image analysis together with a statistical data analysis based on a multivariate, multi-aspect testing approach.

2.Materials and methods

2.1 Mice

A series of 11 NZB/W F1 female mice (22-week-old), purchased from (Harlan Laboratories, Envigo RMS, UD, Italy) and 5 wild type (WT) female mice were housed in the animal facility of the Department of Surgery, Oncology and Gastroenterology of the University of Padova, Padova, Italy. The housing conditions were controlled, with the temperature at 21–23°C and a 12:12 hours light:

dark cycle. All animal studies were approved by the Institutional Animal Care and Use Committee of the Albert Einstein College of Medicine. Mice used in this study were littermates. The NZB/W mice used are hybrid of two inbred strains (NZB females X NZW males) that are genetically uniform and heterozygous only for the genes for which the two parental strains differ. The genetic heterozygosity is related to some dominant alleles wherewith the two parental mice strains contribute in the development of the typical lupus-like auto anti-bodies production. Probably due to estrogen action and as it's observed in human, lupus syndrome in the NZB/W F1 strain is strongly biased in favor of female

2.2 Assessment of lupus

Mice were monitored twice a week for the development of proteinuria and autoantibody titers. Urinary protein excretion was measured by dipstick analysis (Uristix; Bayer), where +1 is 30 mg/dl, +2 is 100 mg/dl, +3 is 300 mg/dl, and +4 is ≥2000 mg/dl (supplementary material Table 1). Active generalized SLE was present in all mice of the NZBW group, as determined by elevated serum anti-DNA antibodies and by the presence of glomerulonephritis. Mouse IgG anti-double stranded (ds) DNA antibody titers were determined by ELISA, as previously described in detail (Gatto et al., 2016; Gatto et al., 2020). Similar ELISA protocols were also used for anti-chromatin, anti-cardiolipin and anti-N-methyl-D-aspartate receptor antibody ELISAs (Gatto et al., 2016; Gatto et al., 2020). For details of weight, age, values of proteinuria and autoantibody titers analyzed in NZBW mice before death see (supplementary material Table 1).

2.3 Brain tissue preparation and Nissl staining

The mouse brains were fixed in a 10% formaldehyde solution. After fixation, the brains were processed for paraffin embedding. The brains were cut into 8-µm-thick coronal sections. From each sample, continuous brain sections were stained following a routine Nissl protocol (Corain et al., 2020). The topography of the hippocampal region was assessed by comparison with detailed stereotaxic mouse brain atlases (Paxinos and Franklin, 2012). For cytoarchitectural analysis of the

hippocampus we selected the range from Bregma was from -2.80 mm to -3.40 mm. In order to evaluate the hippocampal regions extension, we Nissl stained one section every ten per mouse brain in both NZB/WF1 and wild type populations.

2.4 Image acquisition and topographical mapping of the hippocampal subregions

Nissl-stained sections were digitalized with a semi-automated microscope (D-Sight v2, Menarini Diagnostics, Italy) with the 20x objecive at the best focal plane. The layers of interest were manually segmented on each acquired image using a general-purpose image-editing software (GNU Image Manipulation Program, The GIMP Development Team, 2019). For details see (supplementary material, Figure 1).

2.5 Automatic cell identification

Each neuron was identified and segmented through an automatic image analysis method applied on the Nissl-stained section (Grisan et al., 2018). The process identified the position and outline of the visible cells within the manually outlined regions. Briefly, a local space-varying threshold applied to the image separated the stained objects (foreground) from the background. From the local surface density of the foreground objects (mainly cells), a separation of the densest (with clustered and cluttered cells) and sparsest regions is obtained (Poletti et al., 2012; Grisan et al. 2018), and the potential cell cluster were then identified. All identified clusters underwent secondary analyses to separate the cells composing them.

2.6 Cells classification by shape type and morphometric descriptors setting

For each cell in each subregion data characterizing its shape and local relationship with surrounding cells were collected (Corain et al., 2020). These data broadly belong to three domains: Size, Regularity and Density (supplementary material, Table 2). Size regarding cell morphology, are composed by shape measurements (area, perimeter, major and minor axis length). Regularity

delineate the domain that consider the parameter Extent and the parameters Solidity. Extent is defined as: Area / (Area of the bounding box); Solidity is defined as the proportion of the pixels in the convex hull that are also in the object; computed as Area/Convex Area. We defined "more regular" the neurons showing values closer to 1 of Extent and Solidity (cells show a rounded shape) in comparison to the lower values of these parameters (cells tend to be farther from the round shape). Density characterizes the context neighboring each cell by counting the number of cells within a radius of 50 µm or within 100 µm from the cell under analysis. Density descriptors are an absolute number of neighbor cells around a given cell. All neural cells were grouped in 4 categories defined by their shape: pyramidal, round, ellipsoid and complex. The total number of cells analyzed for the NZBW mice population and for the Wild Type mice population, in each subregions separately for cell shape is reported in the supplementary material. For details see (supplementary material, Table 2, Table 3 and Figure 2).

2.7 Statistical Analysis

The statistical analysis was performed comparing WT and NZBW populations for each domain within the 7 layers and the 4 shape types. As multiple cells recorded in each image are not independent, resampling-based the method proposed by (Finos and Basso, 2012) was used to account for repeated measures. The method is as follows: each image the mean of each feature is computed and used as pseudo-observation. The pseudo-observations are now independent, but not homoscedastic. They are randomly permuted among groups, while an adequate test statistics accounts for the heteroscedasticity. The p-value is the proportion of test statistics computed on randomly permuted pseudo-observations that exceeds the one computed on observed data.

This approach takes into account the joint distribution of the tests and allows for the multivariate inference via nonparametric Fisher combination of the univariate test. The tests are combined by morphometric descriptors, subregion and cell type. Significance level was set to alpha=0.05. The analysis was performed with R software (R Core Team, 2021) and flip package (Finos, 2018). For

descriptive purposes, a Principal Component Analysis was performed for each layer after standardization of the morphometric descriptors. A bi-plot of the first two principal components was drawn also reporting the explained variance of each component.

3. Results

3.1 Lamination of the hippocampal region and subregion

The DG, CA1, CA2 and CA3 regions were identified as well as the 7 subregions PoDG, Or, Py, Rad, LMol, MoDG and GrDG and their cytoarchitecture, in all mice (Figure 1). Within each subregion, the 4 categories of cells type (pyramidal, round, ellipsoid and complex) were found in both NZBW and WT population. The general anatomy of the hippocampus followed its well-known description (Figure 1).

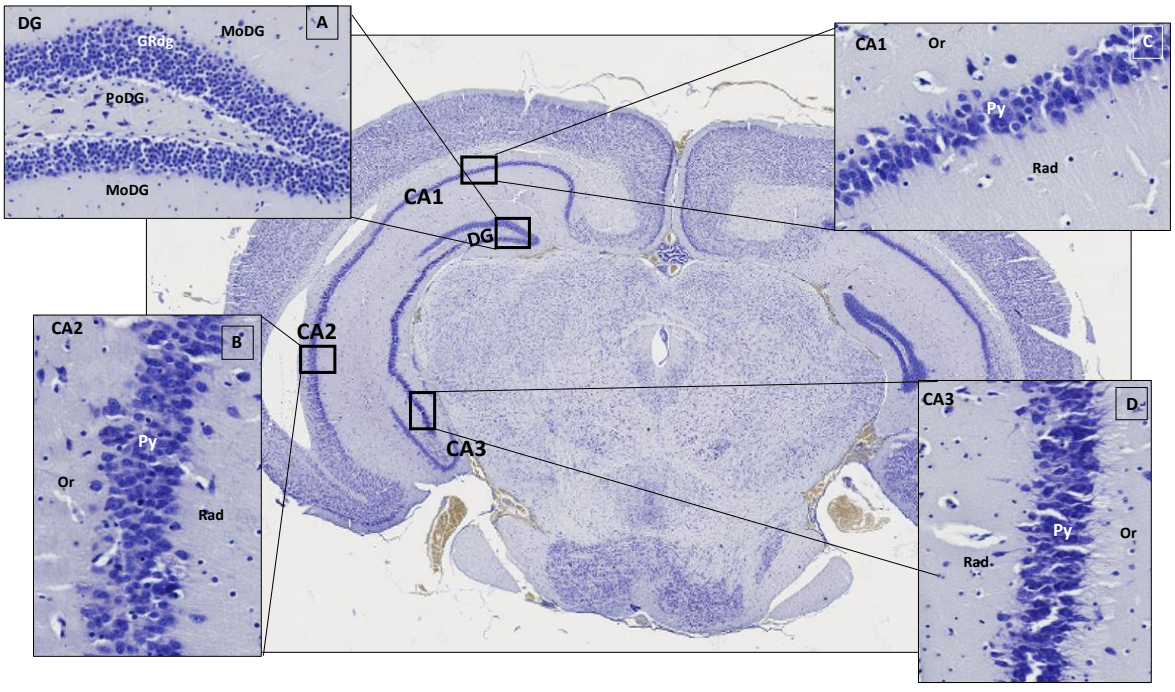

Figure 1: A. Image of a Nissl stained coronal section of WT mouse brain showing the Dg, CA1, CA2 and CA3 hippocampal regions (X20). **A.** Enlargement of DG showing details of neuronal cells in the PoDG, GrDG and MoDG subregions. **B.** Enlargement of CA2 region showing details of neuronal cells in the Py, Or and Rad subregions. **C.** Enlargement of CA1 region showing details of neuronal cells in the Or, Py, Rad, subregions. **D.** Enlargement of CA3 region showing details of neuronal cells in the Py, Or and Rad subregion.

201

202 *3.2 Neurons in the NZBW hippocampus showed larger body size than WT neurons.*

203 The cells in the hippocampal neurons of NZBW mice were larger than neurons of WT mice in all
204 subregions (Figure 2). The Py subregion, where neurons had a larger perimeter in WT than NZBW
205 mice, was an exception. Representation of the results, separately for each morphometric descriptor
206 are shown in Figure 2. Inferential analysis demonstrated a strongly statistically significant difference
207 ($p \leq 0.01$) in NZBW mice in the PoDG, Or, Py, Rad subregions, and a statistically significant
208 difference ($p \leq 0.05$) in the GrDG and LMol subregions (Table 1). No difference in the size of neurons
209 was found in the MoDg or the GrDG subregion. The analysis performed by categories and by
210 subregion revealed which cell shape type contributed to the statistical significance (Table 1).
211 Details of the mean difference and standard error are reported separately for each morphometric
212 descriptor in the section "Additional statistical results, (supplementary material). Moreover, detailed
213 results of the p-values combined for domains subregions, cell shape and morphometric descriptor are
214 reported in the in the section "Additional statistical results", (supplementary material).

215

Subregion	cell population Size difference p-value				
	Whole subregion	Round cells	Ellipsoid cells	Pyramidal cells	Complex cells
PoDG	0.0020	0.0030	0.0020	0.0010	0.0410
Or	0.0020	0.0020	0.0010	0.0030	0.0450
Py	0.0080	0.0040	0.0040	0.0020	0.1550
Rad	0.0050	0.0670	0.0020	0.0150	0.0090
LMol	0.0410	0.1530	0.0040	0.0290	0.9530
MoDG	0.0570	0.1530	0.0040	0.0290	0.9530
GrDG	0.0150	0.0010	0.0130	0.1120	0.0200

Table 1: significant p-value combined by subregion and cells shape type for the domain Size with adjustment by multiplicity. The 1% statistically significant p-values are highlighted in bold.

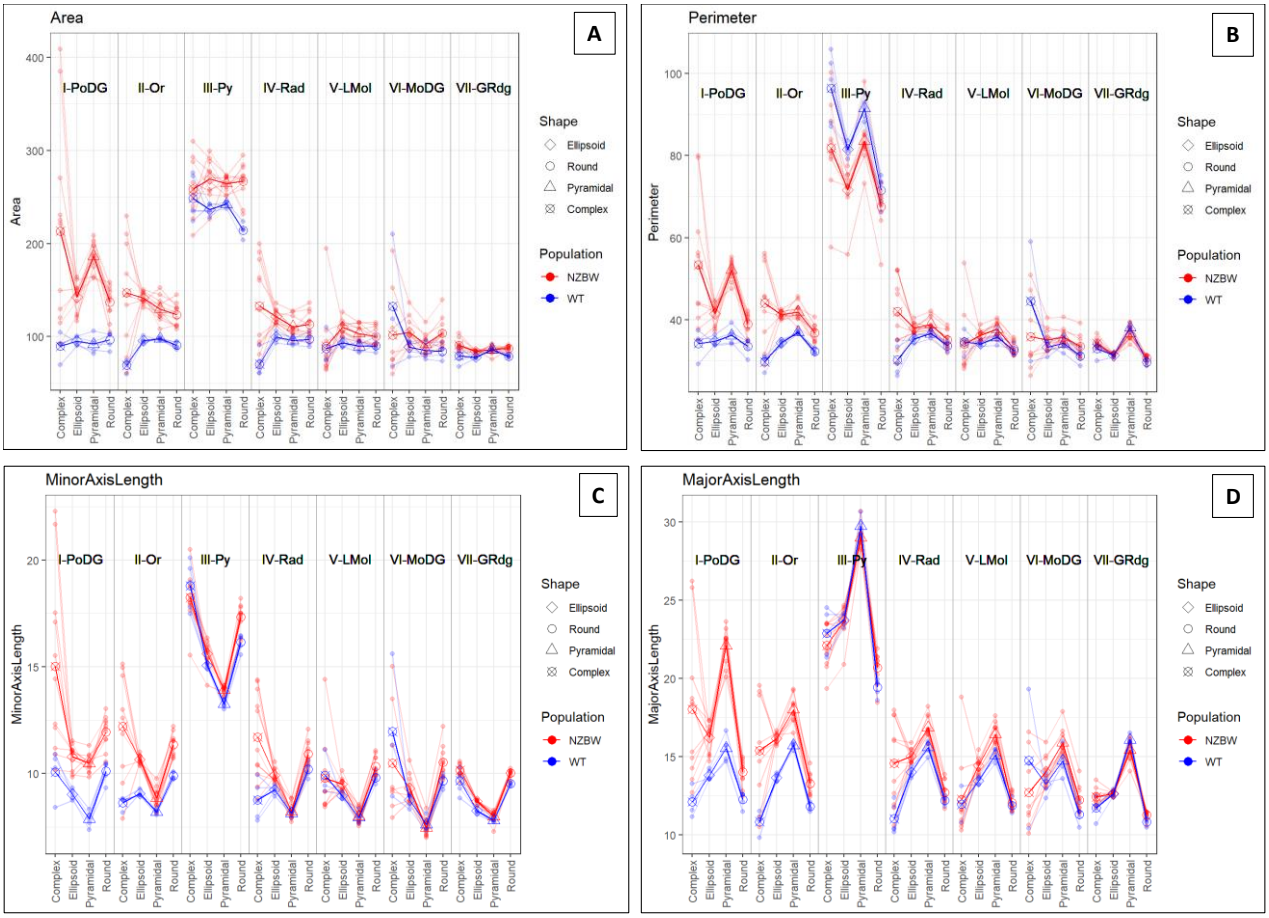

Figure 2: Graphical representation of the Size morphometric descriptors. Results are presented by subject and by subregion, separately per cell shape types, in the two populations NZBW (red lines) and WT (blue lines). In **A,** plot of the area (in micons^2). In **B,** plot of the perimeter (micons). In **C,** plot of minor axis length. The parameter "minor axis length" corresponds to the length of the minor axis of the cell body expressed in µm. In **D,** plot of major axis length. The parameter major axis length corresponds to the length of the major axis of the cell body expressed in µm. The mean values for each morphometric descriptor are reported for the NZBW mice (red bold line) and for the WT mice (blue bold line).

3.3 WT mice showed a distinct clustering compared to NZBW for the domain Size

The principal components analysis score plot was applied to visualize the sample distribution patterns (Figure 3). The two-dimensional scatter plot was defined by the first and second principal components

(PC1 and PC2, respectively). In all subregions except the MoDG, the NZBW mice were clearly separated from WT. In the PoDg, OR Py Rad and LMol subregions, the PC1 and 2 accounted for > 80% of the total variance, indicating that WT subjects were well distinguished from NZBW, accounting for a large part of the statistically significant differences between them (Figure 3).

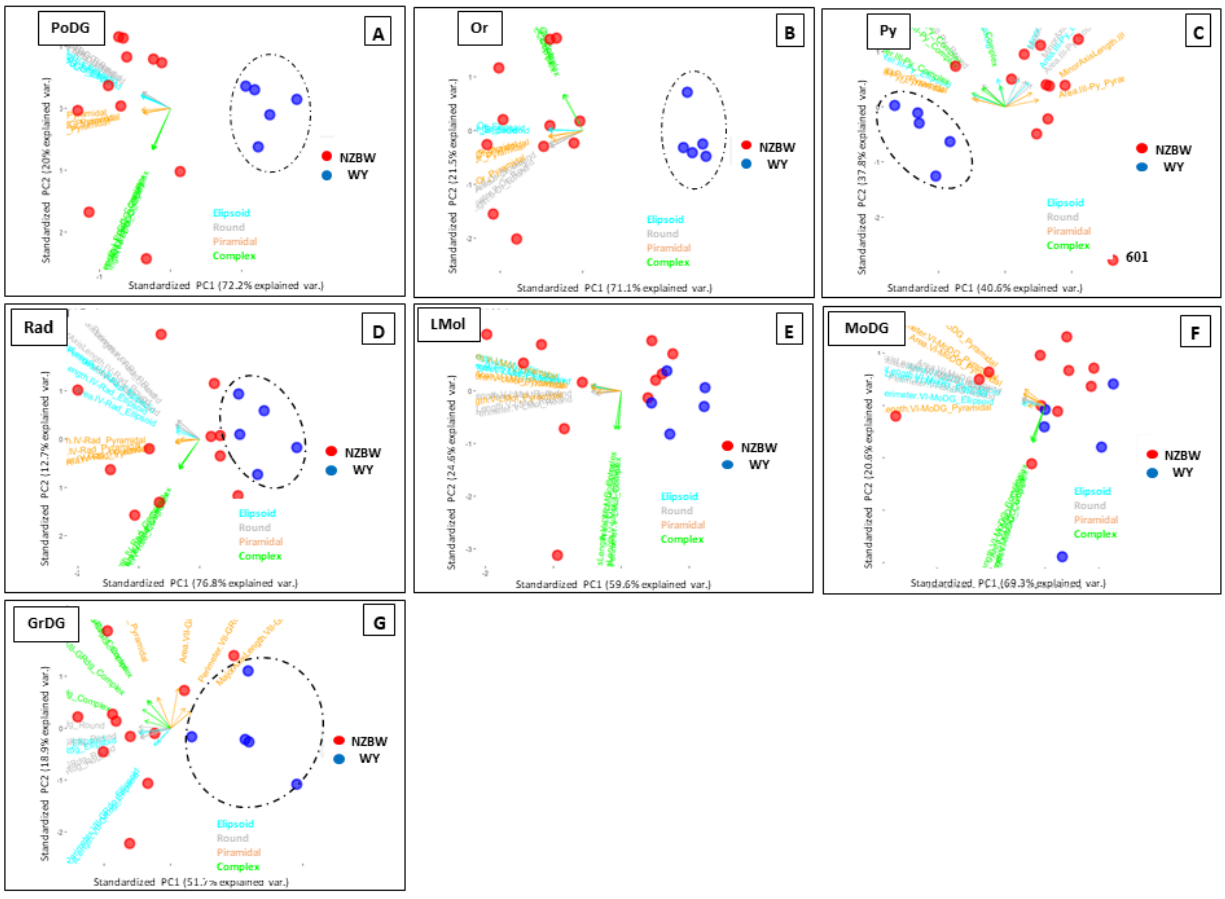

Figure 3: plot of the first (x-axis) against second (y-axis) PCA, for the Size domain, separated for each subregion, showing similarities (closer points) and differences (distant points) between each of the subjects bi-dimensionally separately for hippocampal subregion: in the plot **A** the PoDG; in **B** the Or, in **C** the Py, in **D** the Rad, in **E** the LMol, in **F** the MoDG, in G the GrDG. Each data point corresponds to one subject in function of the first two principal components of the morphometric descriptors. The single subjects resulted grouped by multiple inter-correlated variables and for the four types of cells shape considered (light blue, green, gray and yellow color). NZBW mice (red dots) and WT mice (blue dots).

3.4 Neurons in the hippocampus of NZBW mice showed more regular cell shape than WT neurons.

The results for the Regularity morphometric descriptors revealed that NZBW neurons were more regular ($p \leq 0.01$) than WT neurons in all subregions (Figure 4).

Inferential results obtained separately for each shape type revealed that round, ellipsoid and pyramidal cell contributed strongly ($p \leq 0.01$) to the statistical difference, while the complex shape type did not show differences (Table 2). Again, graphically, the Py neurons seemed to differ more between them and across cell shape.

Subregion	cell population Regularity difference p-value				
	Whole subregion	Round cells	Ellipsoid cells	Pyramidal cells	Complex cells
PoDG	0.0010	0.0010	0.0010	0.0040	0.3570
Or	0.0010	0.0010	0.0030	0.0010	0.5070
Py	0.0010	0.0140	0.0010	0.0010	0.0840
Rad	0.0010	0.0010	0.0040	0.0010	0.8310
LMol	0.0010	0.0010	0.0010	0.0010	0.2690
MoDG	0.0010	0.0030	0.0030	0.0010	0.0900
GrDG	0.0010	0.0250	0.0510	0.0510	0.2490

Table 2: statistically significant p-value combined by subregion and cells shape type for the Regularity domain with adjustment by multiplicity. The 1% statistically significant p-values are highlighted in bold.

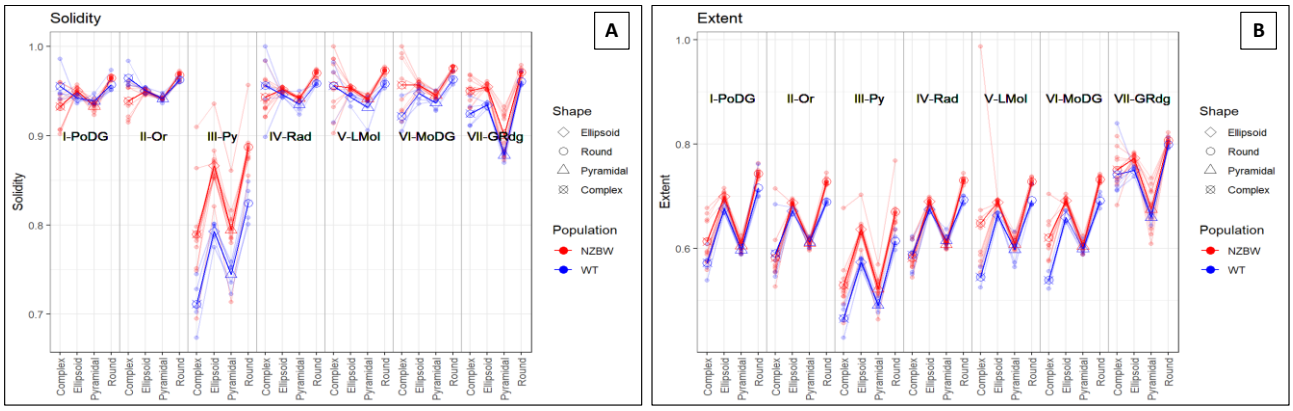

Figure 4: Graphical representation of the Regularity morphometric descriptors solidity (plot A) and extent (plot B). Results are described by subject and by subregion, separately per cell shape types; NZBW (red lines) and WT (blue lines). The mean value for each morphometric descriptor is reported for the NZBW mice (red bold line) and for the WT mice (blue bold line).

3.5 Principal component analysis of NZBW populations and WT populations for the Regularity domain

In all subregions, the PCA demonstrated a clear segregation of the WT and NZBW populations (Figure 5). In Rad, PoDG but most prominently in Lmol and MoDG, the NZBW were closely clustered while WT were more widely distributed. In the Or and Py subregions, WT subjects formed a homogeneous group, while the subjects of the NZBW population exhibited a much wider distribution.

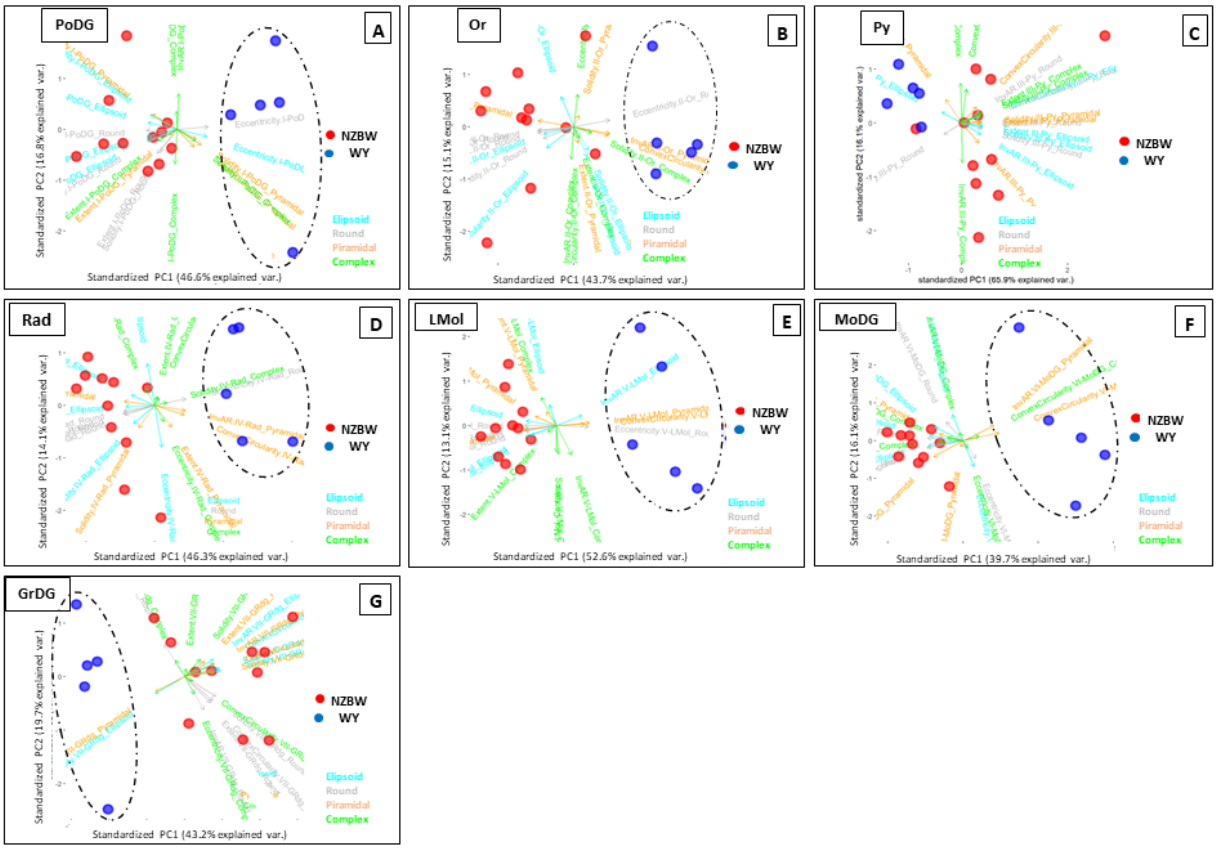

Figure 5: plot of the first (x-axis) against second (y-axis) PCA, for the Regularity domain, separated for each subregion, showing similarities (closer points) and differences (distant points) between each of the subjects bi-dimensionally: in the plot **A** the PoDG; in **B** the Or, in **C** the Py, in **D** the Rad, in **E** the LMol, in **F** the MoDG, in G the GrDG. Each data point corresponds to one subject in function of the first two principal components of the morphometric descriptors. The single subjects resulted grouped by multiple inter-correlated variables and for the four types of cells shape considered (light blue, green, gray and yellow color). NZBW mice (red dots) and WT mice (blue dots).

3.6 Neurons in the hippocampus of NZBW mice were denser than neurons in WT

NZBW neurons were denser than WT in most cases, except in Py and GrDG subregion (Figure 6). The NZBW mice presented higher cell density in the Or, Rad, LMol and MoDG than the WT mice (Figure 6). Multivariate analysis indicated a strong statistically significant difference ($p \leq 0.01$) in the Py, Rad LMol and MoDG, and statistically significant in Or ($p \leq 0.05$), (Table 3).

Interestingly, the density in the Py subregion was lower in NZBW than in WT, and that was true for all the cell shape types (Figure 6). The PoDG and GrDG subregions did not significant variation in cells density between the two mice populations (Table 3). In MoDg, Or and Lmol, the complex shapes were not significantly different from WT; neither were the pyramidal cells in MoDG.

Subregion	cell population Density difference p-value				
	Whole subregion	Round cells	Ellipsoid cells	Pyramidal cells	Complex cells
PoDG	0.2330	0.5490	0.4430	0.0550	0.2350
Or	0.0240	0.0200	0.0110	0.0070	0.2210
Py	0.0090	0.0030	0.0040	0.0080	0.0190
Rad	0.0080	0.0030	0.0040	0.0080	0.0080
LMol	0.0090	0.0020	0.0020	0.0020	0.6990
MoDG	0.0090	0.0060	0.0020	0.0020	0.1410
GrDG	0.2330	0.1530	0.0960	0.4110	0.0960

Table 3: statistically significant p-value combined by subregion and cells shape type for the Density domain with adjustment by multiplicity. The 1% statistically significant p-values are highlighted in bold.

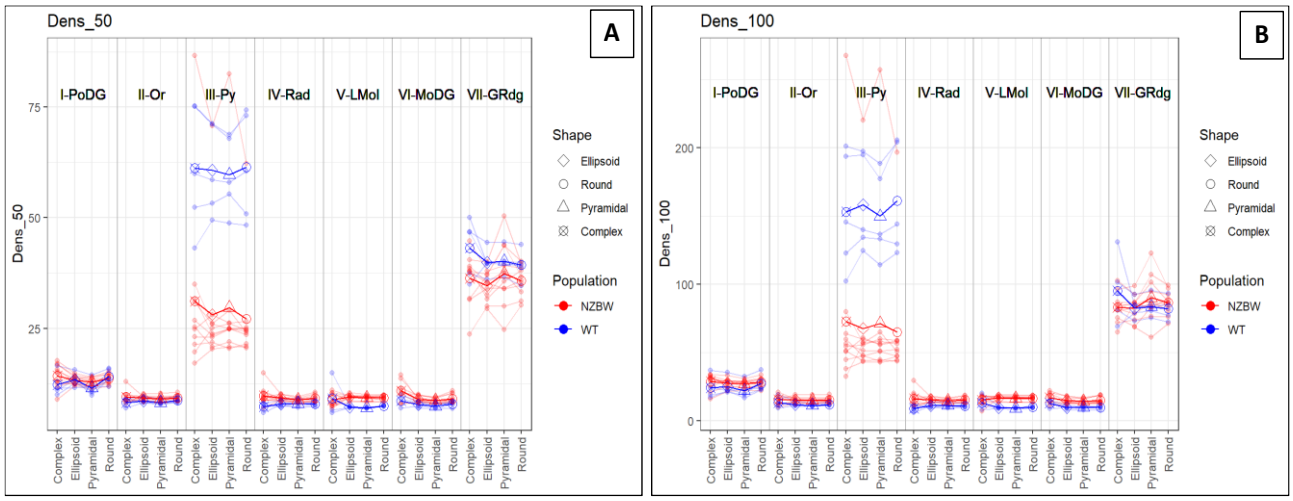

Figure 6: Graphical representation of the morphometric descriptors Ngb_50 (plot A) and Ngb_100 (plot B), belonging to the Density domain. Results are described by subject and by subregion, separately per the cell shape types; NZBW (red lines) and WT (blue lines). The mean value for each morphometric descriptor is reported for the NZBW mice (red bold line) and for the WT mice (blue bold line).

3.7 Principal component analysis of NZBW populations and WT populations for the Density domain

The PCA showed that, in Py and Lmol, NZBW mice formed a very homogeneous group while WT subjects revealed a more spread-out distribution (Figure 7).

The subjects of the NZBW population in the Py subregion formed a well-defined group (Figure 7). Control mice were homogeneous and close to each other in the Py, Lmol and MoDG. The two groups were clearly demarcated in the context of the Py, the Lmol and relatively so in the MoDG where the PC1 explained 97.5%, 74.6% and 78.2% of the variance, respectively. This was not the case in PoDG, Or, Rad and GrDG, (Figure 7). In Py and Lmol specifically, the two populations seemed most segregated.

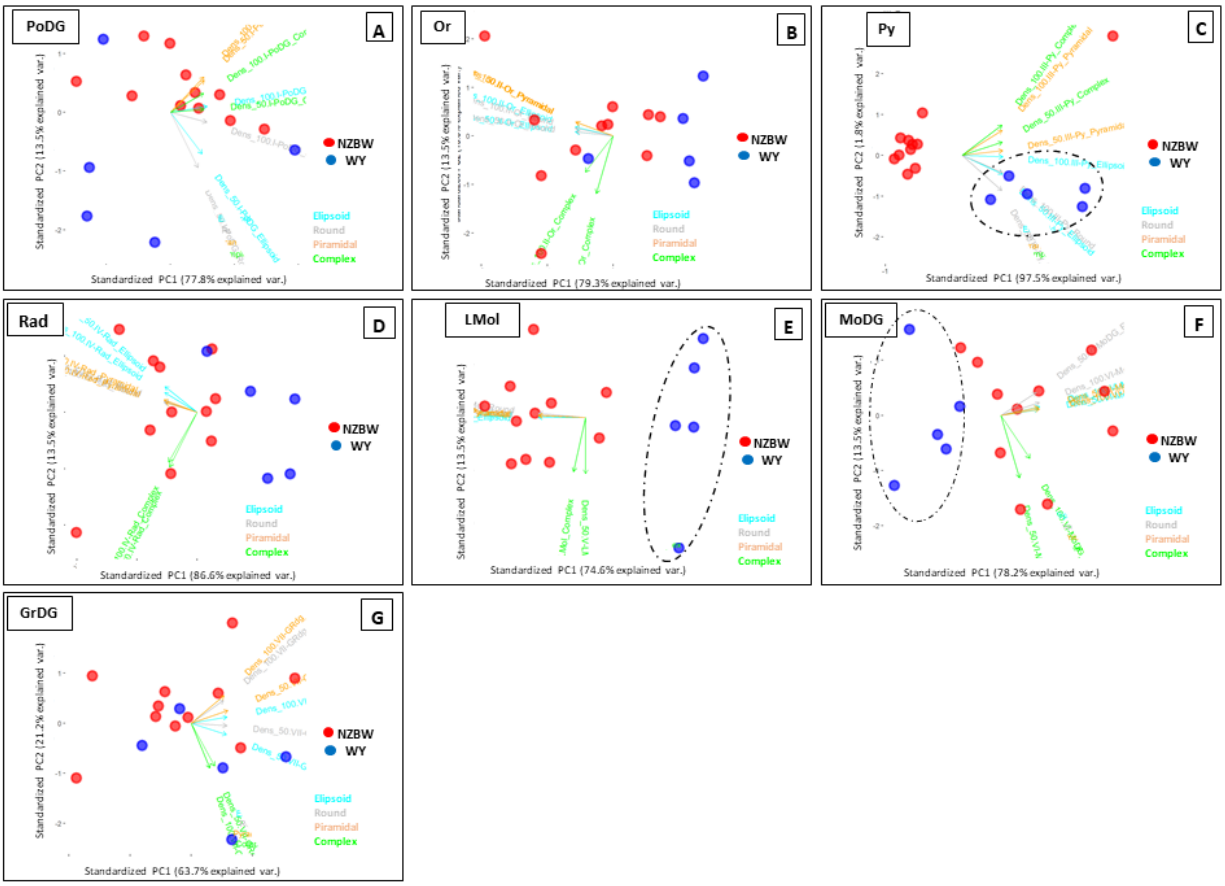

Figure 7: plot of the first PCA versus the second, for the Density domain, showing the be-dimensional visualization of similarities and differences between each of the subjects. Each point corresponds to one subject with a 2-D (the first two principal components) projection of the morphometric descriptors. The single subjects resulted grouped by multiple inter-correlated variables and for the four types of cells shape considered (light blue, green, gray and yellow color). NZBW mice (red dots) and WT mice (blue dots).

3.8 Summary of results

- **Size**: NZBW hippocampal neurons were larger in size than those of WT. No differences were found in the MoDg and GrDG subregion.
- **Regularity**: NZBW hippocampal neurons were significantly more regular than those of WT mice in all the subregions. However, the complex cell shape did not contribute to the statistical significance in any subregion.
- **Density**: In NZBW, neurons were usually denser than in WT. Interestingly, Py neurons were much denser in WT than in NZBW. The PoDG and GrDG did not show difference in cell density.

4.Discussion

This study is aimed at investigating alterations in the internal hippocampal cytoarchitecture of the NZBW mice lupus model. Our results revealed that neurons in the hippocampus of NZBW mice were denser, larger and showed a more a regular cell body than WT mice, apart in the Py subregion, where density of NZBW neurons was lower than in WT. Finally, PCA allow to distinguish healthy WT subjects from NZBW subjects.

4.1 How does NPSLE *induce hippocampal damage? Two alternative hypotheses*

The studies performed on possible hippocampal damages in both human SLE patients and in lupus mice models highlighted two alternative hypotheses: one suggests that NPSLE induces hippocampal damage and atrophy by either reducing the number of neurons (Ballok et al 2004) or reducing the volume of the hippocampal structures (Appenzeller et al., 2006, Bódi et al., 2017; Liu et al., 2020). Conversely, the other hypothesis also proposes that NPSLE causes hippocampal damages, but increasing the local volumes, cells hypertrophy, and cells number (Zimmerman et al., 2017). Other works have argued that, regarding the whole brain, volumetric variations do not scale well with alterations in cognitive abilities, and that the total number of neurons appears to be a much more accurate predictor of cognitive ability (Herculano-Houzel, 2011).

Recently, efforts have been focused on the involvement of microglia in NPSLE cognitive dysfunction, revealing an aberrant overexpression of these cells in lupus mice hippocampi (Qiao et al., 2021). Additionally, Grovola and colleagues assessed neuropathological and neuroinflammatory changes in subregions of the dentate gyrus of the pig (Grovola et al., 2020). They found mossy cell hypertrophy with a statistically significant increase in neuron density, specifically in the MoDG, at 7, 30 days and 1-year post brain injury, suggesting that microglial activation after brain injury may play a role in hippocampal circuit and/or synaptic remodeling (Grovola et al., 2020).

Despite contrasting results resulting in two hypotheses, most of these studies provide evidence on the presence of structural abnormalities in the brain linked to NPSLE manifestations. Whether neuron

morphology might be affected and, eventually, which types or groups of neurons may be responsible for the differential effects on cognitive ability remains a subject of debate. The reason behind different and sometime contrasting results (Ota et al 2022) could be related to the fact that no unifying pathophysiological processes has been found in the etiology of NPSLE.

Using advance quantitative imaging and statistical methods, over a large number of cells, we contributed to the discussion with hard evidence, showing as NZBW hippocampus possess cells hypertrophy (denser and larger neurons) than WT mice

This finding support the hypothesis that NPSLE causes hippocampal cells hypertrophy. Conversely, the Py subregion in NZBW mice present lower density than in WT mice supporting the hypothesis that NPSLE induce hippocampal damage by reducing the number of neurons.

4.2 Analysis combined by subregion and by cell shape allowed to highlight hidden differences

We carried out the present analysis separately for the 7 hippocampal subregions, considering 4 types of neuronal shape. Using this focal approach, we were able to identify the hippocampal subregions in which the cytoarchitecture was altered and the type of neurons involved. An accurate account of the internal hippocampal cytoarchitecture is a key step towards the elucidation of the pathogenic mechanisms underlying NPSLE and virtually in all neurological disorders. In this sense the characterization of neuronal morphometry *via* descriptors at the cytoarchitecture meso-scale of an organ or a layer appears to be a powerful indicator of neural cells functions in health *vs.* pathology (Herculano-Houzel, 2011).

4.3 The NZBW mice had larger body size and were denser than WT mice in PoDG, Or, Py, Rad, LMol

The Or, Rad and LMol subregions are relatively cell-free areas containing subpopulations of interneurons. An interesting aspect in the LMol subregions is the presence of specific interneurons type, the so-called neuroglia-form cells that mediate powerful inhibition of CA1 pyramidal cells (Capogna 2011). These interneurons play an important role in the regulation of local circuits in the

hippocampus proper, selectively regulating specific groups of neurons to enhance their function or protect vulnerable neurons from damage (Houser, 2007). Our results show that interneurons density and soma size tended to increase in the Or, Rad and LMol subregions of NZBW mice. Despite the lack of data regarding interneuron morphology of patients with SLE or in lupus mice models, evidence of hypertrophy of interneurons in the hippocampus were described in several neuropathological conditions, including mice after epiloptogenetic hippocampal lesion (Sieu et al., 2017) and in the mouse model for the neurodegenerative disorder's neuronal ceroid lipofuscinoses (Cooper et al., 1999).

Pyramidal neurons are responsible to provide organized responses to spatial stimuli, non-spatial stimuli, and time in the Py subregions (Lisman et al., 2017). An increase in the soma size of the pyramidal neurons associated to cytoplasmic accumulations of phosphorylated neurofilament was demonstrated in neuropathological condition as hippocampal sclerosis in human (Thom et al., 1999). Hypertrophy of the hippocampus associated with an increase in perikarya size of pyramidal neurons was found also in transgenic synRas mice (Gärtner et al., 2004), suggesting an involvement of the Ras-signaling (Rat sarcoma virus) in morpho-regulatory and structural maintenance of hippocampal pyramidal neurons.

In prior works, variation in cell regularity have been considered to evaluate damages in brain areas due to ischemia or to highlight differences in cerebellum of bovine affected from Freemartin syndrome.

Leyh and colleagues, in the murine hippocampus and neocortex analyzed shape and regularity of cells (convex areas, circularities and other parameters) between control hemisphere and ischemic-affected hemisphere. They showed as microglia cells had larger convex hull area and soma circularities, within the control hemisphere compared to the ischemic-affected hemisphere (Leyh et al., 2021).

In a recently work Corain and colleagues set up a method to analyzed the cell shape, regularity and density in bovine cerebellar neurons, to quantify dimorphism in the cytoarchitecture among male,

female and bovine affected from the freemartin syndrome, showing as the Freemartin granule neurons were the largest, most regular and dense (Corain et al., 2020).

4.4 No difference was found in neural density among NZBW and WT mice in the PoDG and GrDG subregion

Differences in neural density between NZBW and WT mice were not significant in the GrDG subregion. A possible explanation of the steady state of granule cells number in NZBW could be the result of the turnover process due to neurogenesis well described in the dentate gyrus of adult mammals (Amaral et al., 2017; Abbott and Nigussie, 2020). Although evidence indicate that neurogenesis in the dentate gyrus persists in the adult mammalian brain and appears to be under environmental control, (Abbott and Nigussie, 2020), studies have shown that the total number of granule cells does not vary in adult animals (Abbott and Gallagher, 1996), demonstrating that there is a steady state turnover of granule cells rather than a continuous accretion. These could explain way no difference was found in GrDG neural density between NZBW and WT mice.

The axons of the excitatory granule neurons in the GrDG reach direct to mossy cells in the PoDG (Scharfman, 2016). The loss of mossy cells, which are excitatory neurons making synaptic contact with granule cells, basket cells, and CA3 pyramidal neurons, has been demonstrated to contribute to DG dysfunction (Scharfman, 2016), resulting in the dysregulation of granule cell excitability, which in turn leads to abnormal behaviors such as anxiety and impaired pattern separation (Jinde et al., 2012).

4.5 WT subjects formed a defined cluster from the scattered NZBW subjects

The PCA analysis grouped the subjects, distinguishing WT subjects from NZBW subjects. Furthermore, it is worth noting that the variability among subjects within NZBW population was much larger than in WT mice.

The variability within NZBW subjects could be mainly due to multisystem involvement and confounding aspects (proteinuria levels) that occur in lupus disease. These multisystem aspects could also be the reason why experimental studies have not yet been able to explain the main causes and mechanisms involved in the pathogenesis of NPSLE (Bruyn, 1995).

The PCA method is useful when data sets from different modalities are combined or if the analysis is complex that there is a need for dimension reduction. Despite is very difficult to clarify how neuroanatomical changes are relating to clinical symptoms of **neurodegenerative diseases**, the PCA showed the possibility to differentiate healthy patients from schizophrenic patients (Caprihan et al., 2008; Rotarska-Jagiela et al., 2008). The application of PCA was proposed also to improve the performance of Alzheimer's disease detection (Halebeedu et al., 2021).

Recently, in the field of SLE, the PCA performed well in in lupus nephritis patients, identifying important risk factors and thus enabling clinicians to identify subjects at-risk and either implement preventative strategies or manage current treatments (Huang et al., 2020). The PCA was also used to determine which groups of cytokines have the greatest influence across disease activity states helping to describe the influence of complex cytokine interactions in SLE (Raymond et al., 2019). The PCA was also applied as a tool to identify lesioned skin patterns in cutaneous lupus erythematosus, helping to characterize where on the body lesions of cutaneous lupus erythematosus tend to occur in patients (Prasad et al., 2020).

The methodology we propose based on in-depth analysis of the morphology of neural cells, provides a collection of valuable data on the morphology of multiple cells, acquired and analyzed individually. In the context of the investigation of pathological changes in structures of the brain areas, due to SLE disease, the application of PCA as technique for reducing the dimensionality of such datasets, allows the increasing interpretability but at the same time minimizing information loss. The collection of large datasets are increasingly common in pathological investigation and the method we proposed could be a powerful tool to distinguish healthy from pathological neurons in postmortem sample analysis.

5.Conclusion

The methodology we set-up consists of multivariate and multi-aspect testing for cytoarchitecture-ranking, based on neuronal cell shape analysis, among populations defined by factors, such as sex, age or pathology. This tool could be a powerful instrument to carry out morphometric analysis providing a robust basis for objective tissue screening, especially in the field of neurodegenerative pathologies.

The analysis carried out separately for each hippocampal subregion provided a baseline to highlight hidden effects on the neuronal cytoarchitecture with respect to analyses conducted without this subdivision.

The application of PCA methodology represents a possible approach to understanding the effects of lupus disease in the brain, optimizing the interpretation of complex data in diagnostics of neurolupus consequences.

Despite the statistically significant morphologic alterations that we found in the NZBW lupus mice hippocampal cytoarchitecture, it remains to be determined whether these structural modifications are associated with the progress of the autoimmune disease and whether these modifications are functionally important.

We are aware that the pathogenetic aspects of lupus in NZBW mice are not entirely representative of the of human pathology. However, this murine model can significantly contribute towards the understanding of lupus.

Abbreviation

NZB/W F1 (NZBW)

Systemic Lupus Erythematosus (SLE)

Central nervous system (CNS)

Neuropsychiatric SLE (NPSLE)

Dentate gyrus (DG),

Molecular layer (MoDG),

Granule cell layer (GrDG)

Polymorph dentate gyrus (PoDG)

Pyramidal layer (Py)

Stratum oriens (Or)

Stratum radiatum (Rad)

Stratum lacunosum-moleculare (LMol)

Declarations:

Ethics approval and Consent to Participate: All experimental procedures were previously approved by the "Padova University Animal Ethic Committee and Italian Ministry of Health with the authorization number 720/2017-PR under the Italian Law Dlgs 26/2014".

Consent to publication: The authors declare that they consent to publication.

Availability of data and material: The authors declare that data and material can be freely given upon request.

Authors' contributions: Antonella Peruffo: Conceptualization, Supervision, Writing, Original draft, Writing - review & editing. Jean-Marie Graïc: Conceptualization, Methodology, Writing - review & editing. Tommaso Gerussi: Methodology, Writing - review & editing. Bruno Cozzi: Conceptualization, Writing - review & editing. Andrea Doria: Conceptualization, Writing - review & editing. Mariella Gatto: Writing - review & editing. Livio Finos: Methodology, Writing - review & editing.. Livio Corain: Methodology, Writing - review & editing. Roberto Luisetto:

Conceptualization, Writing - review & editing. Enrico Grisan: Methodology, Supervision, Writing - review & editing.

Acknowledgements (Not applicable)

References

Abbott LC, Nigussie F. Adult neurogenesis in the mammalian dentate gyrus. Anat Histol Embryol. 2020 Jan;49(1):3-16. doi: 10.1111/ahe.12496. Abramson SB, Amin AR, Clancy RM, Attur M. The role of nitric oxide in tissue destruction. Best Pract Res Clin Rheumatol. 2001. 15:831-45.

Allen TA, Fortin NJ. 2013. The evolution of episodic memory. Proc Natl Acad Sci USA. 110(Suppl):10379–10386.

Amaral DG, Scharfman HE, Lavenex P. The dentate gyrus: fundamental neuroanatomical organization (dentate gyrus for dummies). Prog Brain Res. 2007;163:3-22. doi: 10.1016/S0079-6123(07)63001-5.

Appenzeller S, Carnevalle, Li LM, Costallat LTL, Cendes F. Hippocampal atrophy in systemic lupus erythematosus. Ann Rheum Dis 2006; 65:1585–1589. doi: 10.1136/ard.2005.049486

Ballok DA, Woulfe J, Sur M, Cyr M, Sakic B. Hippocampal damage in mouse and human forms of systemic autoimmune disease. Hippocampus. 2004;14(5):649-61.

Barr ML, Hamilton JD. A quantitative study of certain morphological changes in spinal motor neurons during axon reaction. J Comp Neurol. 1948t;89(2):93-121. doi: 10.1002/cne.900890203.

Belkhelfa M, Beder N, Mouhoub D, Amri M, Hayet R, Tighilt N, Bakheti S, aimouche S, Azzouz D, Belhadj R, Touil-Boukoffa C. The involvement of neuroinflammation and necroptosis in the hippocampus during vascular dementia. J Neuroimmunol. 2018 Jul 15;320:48-57. doi: 10.1016/j.jneuroim.2018.04.004.

Bódi N, Polgár A, Kiss E, Mester Á, Poór G, Kéri S. Reduced volumes of the CA1 and CA4-dentate gyrus hippocampal subfields in systemic lupus erythematosus. Lupus. 2017;26(13):1378-1382. doi: 10.1177/0961203317701845.

Bracci-Laudiero L, Aloe L, Lundeberg T, Theodorsson E, Stenfors C. Altered levels of neuropeptides characterize the brain of lupus prone mice. Neurosci Lett. 1999 Nov 5;275(1):57-60. doi: 10.1016/s0304-3940(99)00737-5.

Briani C, Lucchetta M, Ghirardello A, Toffanin E, Zampieri S, Ruggero S, Scarlato M, Quattrini A, Bassi N, Ermani M, Battistin L, Doria A. Neurolupus is associated with anti-ribosomal P protein antibodies: an inception cohort study. J Autoimmun. 2009 Mar;32(2):79-84. doi: 10.1016/j.jaut.2008.12.002.

Bruyn GA. Controversies in lupus: nervous system involvement. Ann Rheum Dis 1995; 54:159–167.

Capogna M. Neurogliaform cells and other interneurons of stratum lacunosum-moleculare gate entorhinal–hippocampal dialogue. J Physiol. 2011; 589 (Pt 8): 1875–1883. doi: 10.1113/jphysiol.2010.201004.

Caprihan A, Pearlson GD, Calhoun VD. Application of principal component analysis to distinguish patients with schizophrenia from healthy controls based on fractional anisotropy measurements. Neuroimage. 2008; 42(2):675-82. doi: 10.1016/j.neuroimage.2008.04.255.

Cooper JD, Messer A, Feng AK, Chua-Couzens J, Mobley WC. Apparent loss and hypertrophy of interneurons in a mouse model of neuronal ceroid lipofuscinosis: evidence for partial response to insulin-like growth factor-1 treatment. J Neurosci. 1999 Apr 1;19(7):2556-67. doi: 10.1523/JNEUROSCI.19-07-02556.1999.

Corain L, Grisan E, Graïc JM, Carvajal-Schiaffino R, Cozzi B, Peruffo A. Multi-aspect testing and ranking inference to quantify dimorphism in the cytoarchitecture of cerebellum of male, female and intersex individuals: a model applied to bovine brains. Brain Struct Funct. 2020 Dec;225(9):2669-2688. doi:10.1007/s00429-020-02147-x.

Devlin JT, Poldrack RA. In praise of tedious anatomy. NeuroImage. 2007;37(4):1033–1041. doi: 10.1016/j.neuroimage.2006.09.055.

Edstrom JE. Ribonucleic acid changes in the motoneurons of the frog during axon regeneration. J Neurochem. 1959;5:43-9. doi:10.1111/j.1471-4159.1959.tb13331.x. PMID: 13819378.

Fernández-Arjona MDM, Grondona JM, Granados-Durán P, Fernández-Llebrez P, López-Ávalos MD. Microglia Morphological Categorization in a Rat Model of Neuroinflammation by Hierarchical Cluster and Principal Components Analysis. Front Cell Neurosci. 2017 Aug 8;11:235. doi: 10.3389/fncel.2017.00235.

Finos L. flip: Multivariate Permutation Tests. R package version 2.5.0. https://CRAN.R-project.otg/package=flip.

Finos L, and Basso D. Permutation tests for between-unit fixed effects in multivariate generalized linear mixed models. Statistics and Computing. 2014; 24(6), 941-952.

Gao L, Slack M, Barnas JL, McDavid A, Anolik J, Looney RJ. Cell Senescence in Lupus. Curr Rheumatol Rep. 2019 Jan 14;21(2):1. doi: 10.1007/s11926-019-0800-6.

Gärtner U, Alpár A, Reimann F, Seeger G, Heumann R, Arendt T. Constitutive Ras activity induces hippocampal hypertrophy and remodeling of pyramidal neurons in synRas mice. J Neurosci Res. 2004;1;77(5):630-41. doi: 10.1002/jnr.20194.

Gatto M, Ghirardello A, Luisetto R, Bassi N, Fedrigo M, Valente M, Valentino S, Del Prete D, Punzi L, Doria A. Immunization with pentraxin 3 (PTX3) leads to anti-PTX3 antibody production and delayed lupus-like nephritis in NZB/NZW F1 mice. J Autoimmun. 2016;74:208-216. doi: 10.1016/j.jaut.2016.07.002.

Gatto M, Radu CM, Luisetto R, Ghirardello A, Bonsembiante F, Trez D, Valentino S, Bottazzi B, Simioni P, Cavicchioli L, Doria A. Immunization with Pentraxin3 prevents transition from subclinical to clinical lupus nephritis in lupus-prone mice: Insights from renal ultrastructural findings. J Autoimmun. 2020;111:102443. doi: 10.1016/j.jaut.2020.102443.

Ghirardello A, Doria A, Zampieri S, Tarricone E, Tozzoli R, Villalta D, Bizzaro N, Piccoli A, Gambari PF. Antinucleosome antibodies in SLE: a two-year follow-up study of 101 patients. J Autoimmun. 2004 ;22(3):235-40. doi:10.1016/j.jaut.2003.12.005.

Grisan E, Graic J-M, Corain L, Peruffo A (2018) Resolving single cells in heavily clustered Nissl-stained images for the analysis of brain cytoarchitecture. In: 2018 IEEE 15th international symposium on biomedical imaging (ISBI 2018), IEEE, pp 427–430. 10.1109/ISBI.2018.8363608.

Grovola MR, Paleologos N, Wofford KL, Harris JP, Browne KD, Johnson V, Duda JE, Wolf JA, Cullen DK. Mossy cell hypertrophy and synaptic changes in the hilus following mild diffuse traumatic brain injury in pigs. J Neuroinflammation. 2020 Jan 31;17(1):44. doi: 10.1186/s12974-020-1720-0.

Iacono D, O'Brien R, Resnick SM, Zonderman AB, Pletnikova O, Rudow G, An Y, West MJ, Crain B, Troncoso JC. Neuronal hypertrophy in asymptomatic Alzheimer disease. J Neuropathol Exp Neurol. 2008;67(6):578-89. doi:10.1097/NEN.0b013e3181772794.

Jarsky T, Roxin A, Kath WL, Spruston N. Conditional dendritic spike propagation following distal synaptic activation of hippocampal CA1 pyramidal neurons. Nat Neurosci. 2005; 8(12):1667-76.

Jinde S, Zsiros V, Jiang Z, Nakao K, Pickel J, Kohno K, et al. Hilar mossy cell degeneration causes transient dentate granule cell hyperexcitability and impaired pattern separation. Neuron. 2012; 76:1189–200.)

Hainmueller T and Bartos M. Dentate gyrus circuits for encoding, retrieval and discrimination of episodic memories. Nat Rev Neurosci. 2020; 21(3):153-168. doi: 10.1038/s41583-019-0260-z.

Halebeedu Subbaraya Suresha, Srirangapatna Sampathkumaran Parthasarathy. Probabilistic Principal Component Analysis and Long ShortTerm Memory Classifier for Automatic Detection of

631 Alzheimer's disease using MRI Brain Images. JJ. Inst. Eng. India Ser. B. 2021;102(4):807–818.
632 https://doi.org/10.1007/s40031-021-00571-z
633
634 Herculano-Houzel, S. Brains matter, bodies maybe not: the case for examining neuron numbers
635 irrespective of body size. Annals of the New York Academy of Sciences. 2011; 1225:191–199).
636
637 Hernandez-Segura A, Nehme J, Demaria M. Hallmarks of Cellular Senescence. Trends Cell Biol.
638 2018 Jun;28(6):436-453. doi: 10.1016/j.tcb.2018.02.001.
639
640 Ho JW, Burwell RD. 2014. Perirhinal and postrhinal functional inputs to the hippocampus In: Space,
641 time and memory in the hippocampal formation. Vienna: Springer; p. 55–81.
642
643 Huang T, Li J, Zhang W. Application of principal component analysis and logistic regression model
644 in lupus nephritis patients with clinical hypothyroidism. BMC Med Res Methodol. 2020 May
645 1;20(1):99. doi:10.1186/s12874-020-00989-x.
646
647 Kowal C, DeGiorgio LA, Nakaoka T, Hetherington H, Huerta PT, Diamond B, Volpe BT. Cognition
648 and immunity; antibody impairs memory. Immunity. 2004; 21(2):179-88. doi:
649 10.1016/j.immuni.2004.07.011.
650
651 Leyh J, Paeschke S, Mages B, Michalski D, Nowicki N, Bechmann I and Winter K. Classification of
652 Microglial Morphological Phenotypes Using Machine Learning. Front Cell Neurosci. 2021; 15:
653 701673. doi: 10.3389/fncel.2021.701673
654

655 Leung JW, Lau BW, Chan VS, Lau CS, So KF. Abnormal increase of neuronal precursor cells and
656 exacerbated neuroinflammation in the corpus callosum in murine model of systemic lupus
657 erythematosus. Restor Neurol Neurosci. 2016;34(3):443-53. doi: 10.3233/RNN-160638.
658
659 Lisman J, Buzsáki G, Eichenbaum H, Nadel L, Ranganath C, Redish AD. Viewpoints: how the
660 hippocampus contributes to memory, navigation and cognition. Nat Neurosci. 2017; 20(11):1434-
661 1447. doi: 10.1038/nn.4661.
662
663 Liu S, Cheng Y, Zhao Y, Lai A, Lv Z, Xie Z, Upreti B, Wang X, Xu X, Luo C, Yu H, Shan B, Xu L,
664 Xu J. Hippocampal Atrophy in Systemic Lupus Erythematosus Patients without Major
665 Neuropsychiatric Manifestations. J Immunol Res. 2020; 2020:2943848. doi: 10.1155/2020/2943848.
666
667 McIlwain DL, Hoke VB. The role of the cytoskeleton in cell body enlargement, ncreased nuclear
668 eccentricity and chromatolysis in axotomized spinal motor neurons. BMC Neurosci. 2005;6:19. doi:
669 10.1186/1471-2202-6-19.
670
671 Merino-Serra P., Tapia-Gonzalez S., DeFelipe J. Calbindin immunostaining in the CA1 hippocampal
672 pyramidal cell layer of the human and mouse: A comparative study. 2020; Journal of Chemical
673 Neuroanatomy. 104: 101745. doi.org/10.1016/j.jchemneu.2020.101745.
674
675 Miller M.A. and Zachary J.F. Mechanisms and Morphology of Cellular Injury, Adaptation, and
676 Death. Pathologic Basis of Veterinary Disease. 2017; 2–43.e19.doi: 10.1016/B978-0-323-35775-
677 3.00001-1
678

679 Ota Y, Srinivasan A, Capizzano AA, Bapuraj JR, Kim J, Kurokawa R, Baba A, Moritani T. Central
680 Nervous System Systemic Lupus Erythematosus: Pathophysiologic, Clinical, and Imaging Features.
681 Radiographics. 2022; 42(1):212-232. doi: 10.1148/rg.210045.
682
683 Paxinos G and Franklin K. Paxinos and Franklin's the Mouse Brain in Stereotaxic Coordinates. Third
684 edition. 2012.
685
686 Pikman R, Kivity S, Levy Y, Arango MT, Chapman J, Yonath H, Shoenfeld Y, Gofrit SG.
687 Neuropsychiatric SLE: from animal model to human. Lupus. 2017. 26:470-477.
688
689 Poletti E, Zappelli F, Ruggeri A, Grisan E. A review of thresholding strategies applied to human
690 chromosome segmentation. Comput Methods Programs Biomed. 2012;108(2):679–688. doi:
691 10.1016/j.cmpb.2011.12.003.
692
693 Prasad S, Raman J, Ogunsanya ME, Chong BF. Principal components analysis as a tool to identify
694 lesional skin patterns in cutaneous lupus erythematosus. J Am Acad Dermatol. 2020 Sep;83(3):922-
695 924. doi: 10.1016/j.jaad.2020.01.010.
696
697 Qiao X, Wang H, Lu L, Chen J, Cheng Q, Guo M, Hou Y, Dou H. Hippocampal microglia CD40
698 mediates NPSLE cognitive dysfunction in mice. J Neuroimmunol. 2021; 357:577620. doi:
699 10.1016/j.jneuroim.2021.577620.
700
701 Ranganath C, Ritchey M. 2012. Two cortical systems for memory-guided behaviour. Nat Rev
702 Neurosci. 13:713–726.
703

704 Rapp PR, Gallagher M. Preserved neuron number in the hippocampus of aged rats with spatial
705 learning deficits. Proc Natl Acad Sci U S A. 1996; 93(18):9926-30. doi: 10.1073/pnas.93.18.9926.
706
707 Raymond WD, Eilertsen GØ, Nossent J. Principal component analysis reveals disconnect between
708 regulatory cytokines and disease activity in Systemic Lupus Erythematosus. Cytokine. 2019;114:67-
709 73. doi: 10.1016/j.cyto.2018.10.013.
710
711 Rotarska-Jagiela A, Schonmeyer R, Oertel V, Haenschel C, Vogeley K, Linden DE. The corpus
712 callosum in schizophrenia-volume and connectivity changes affect specific regions. Neuroimage
713 2008;39:1522–1532.
714
715 Scharfman HE. The enigmatic mossy cell of the dentate gyrus. Nat Rev Neurosci. 2016;17:562–75
716
717 Schnider A, Bassetti C, Schnider A, Gutbrod K, Ozdoba C. Very severe amnesia with acute onset
718 after isolated hippocampal damage due to systemic lupus erythematosus. J Neurol Neurosurg
719 Psychiatry. 1995;59(6):644-6. DOI: 10.1136/jnnp.59.6.644-a.
720
721 Schwartz N, Stock AD, Putterman C. Neuropsychiatric lupus: new mechanistic insights and future
722 treatment directions. Nat Rev Rheumatol. 2019;15(3):137-152. doi: 10.1038/s41584-018-0156-8.
723
724 Sieu LA, Eugène E, Bonnot A, Cohen I. Disrupted Co-activation of Interneurons and Hippocampal
725 Network after Focal Kainate Lesion. Front Neural Circuits. 2017; 11:87. doi:
726 10.3389/fncir.2017.00087.
727
728 Thom M, D'Arrigo C, Scaravilli F. Hippocampal sclerosis with hypertrophy of end folium pyramidal
729 cells. Acta Neuropathol. 1999; 98(1):107-10. doi:10.1007/s004010051057.

730

731 Zaletel I, Filipović D, Puškaš N. Chronic stress, hippocampus and parvalbumin-positive interneurons:
732 what do we know so far? Rev Neurosci. 2016. 27:397-409.

733

734 Zimmermann N, Goulart Corrêa D, Tukamoto G, Netto T, Batista Pereira D, Paz Fonseca R,
735 Gasparetto EL. Brain morphology and cortical thickness variations insystemic lupus erythematosus
736 patients: Differences among neurological, psychiatric, and non-neuropsychiatric manifestations. J
737 Magn Reson Imaging. 2017l;46(1):150-158. doi: 10.1002/jmri.25538.

738

Figure 1

Click here to access/download;Figure;Figure 1.jpg

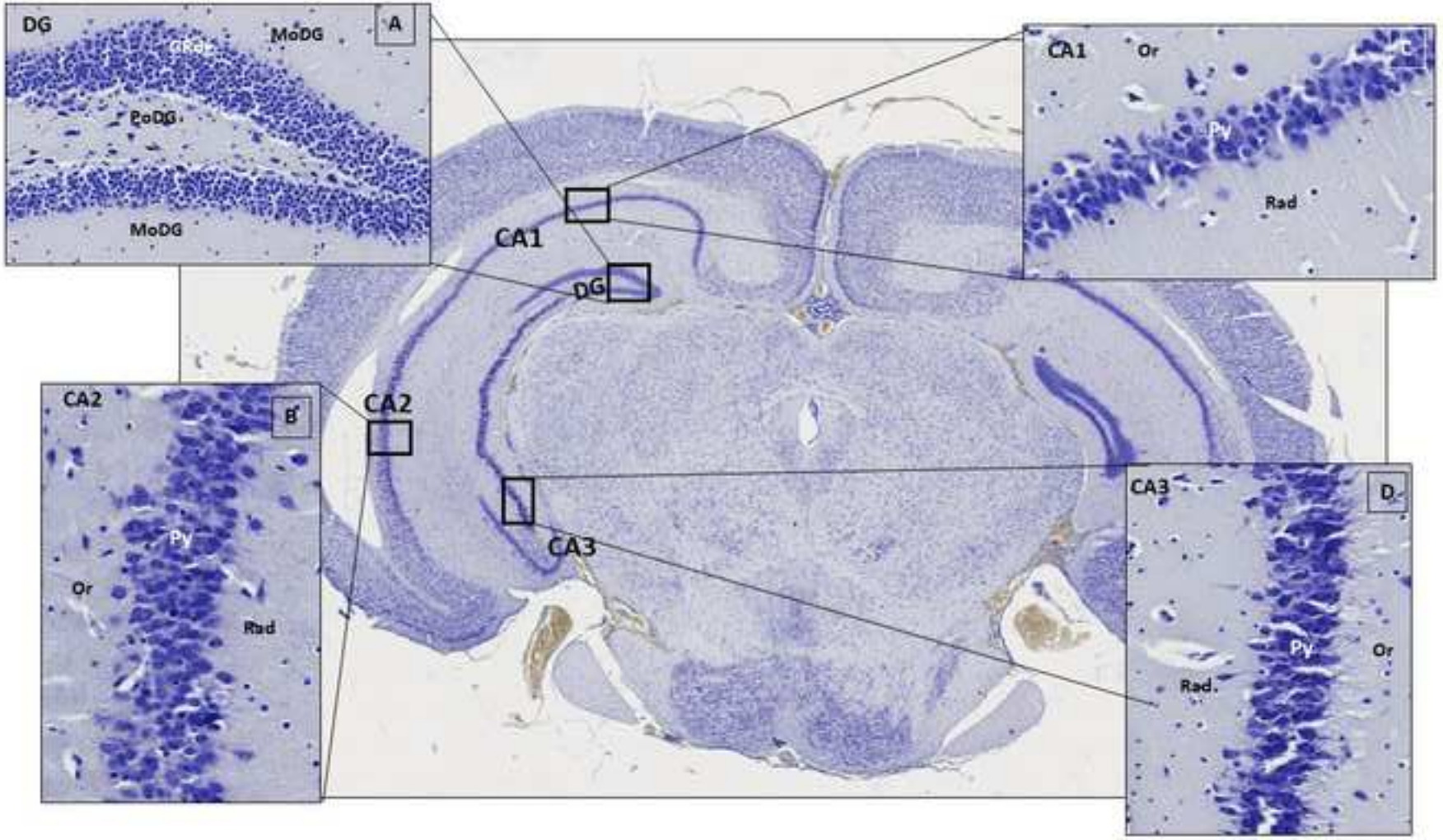

Figure 2

Click here to access/download;Figure;Figure 2.jpg

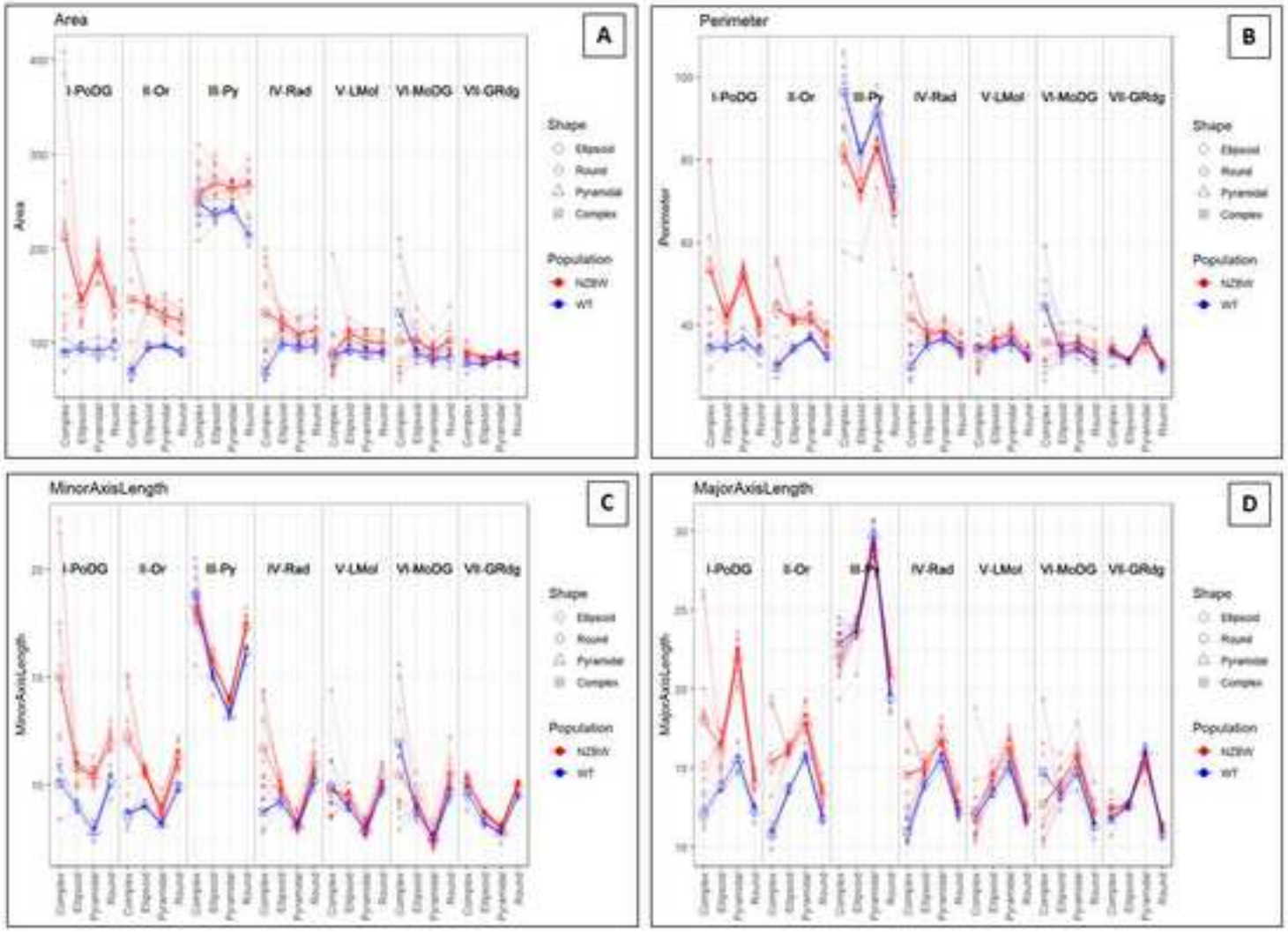

Figure 4

Click here to access/download;Figure;Figure 4.jpg

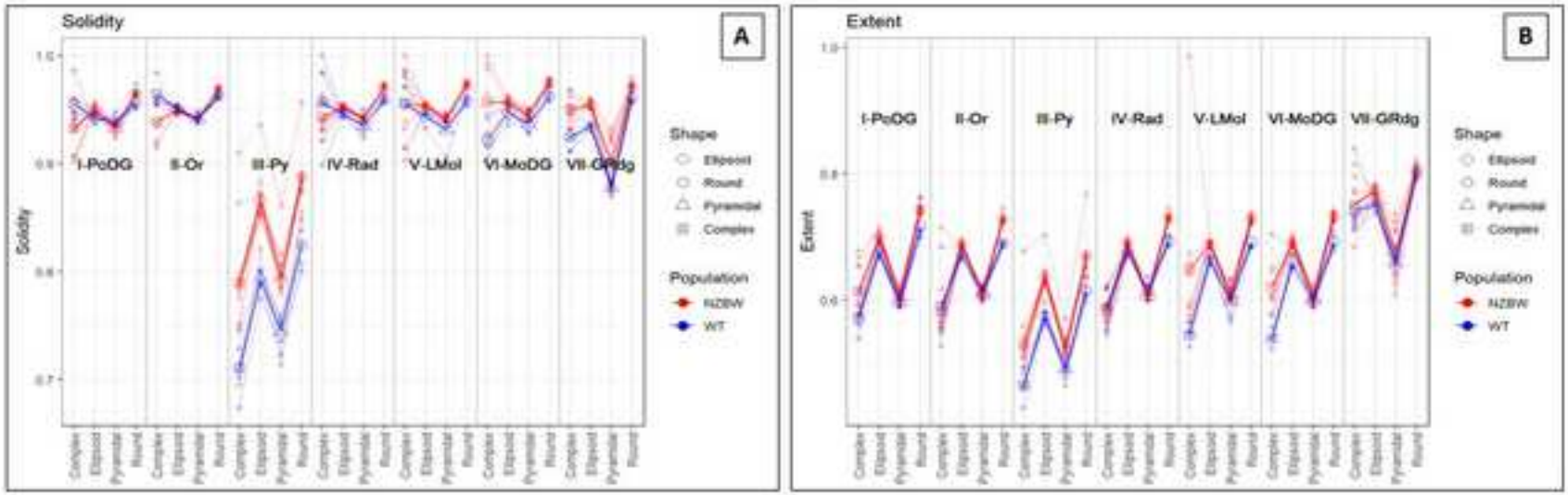

Figure 6

Click here to access/download;Figure;Figure 6.jpg

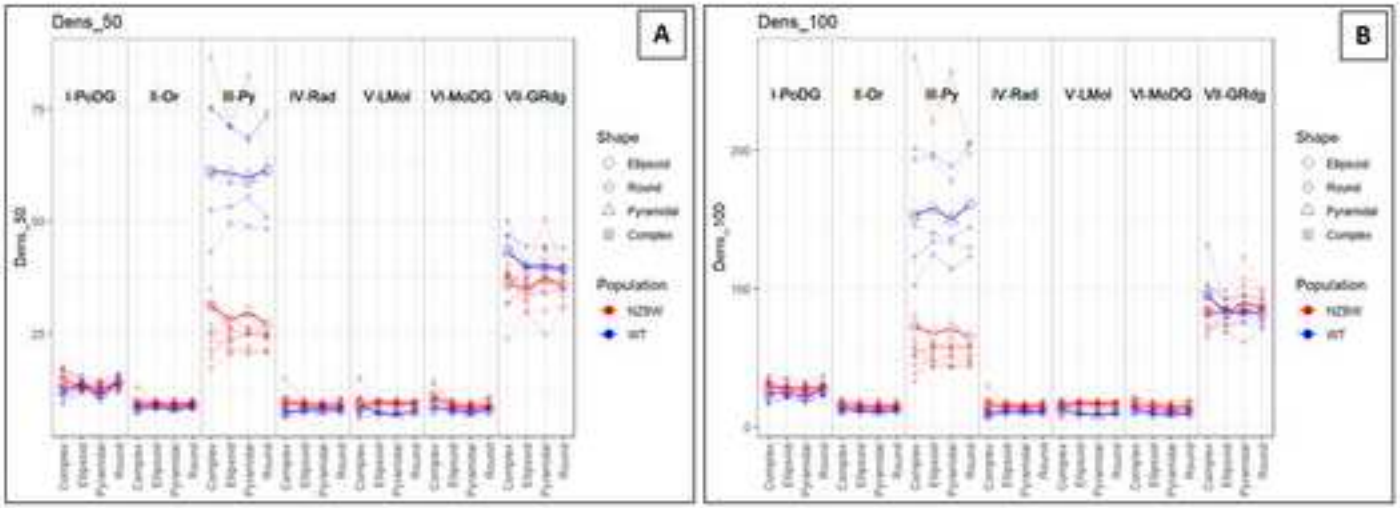

Figure 3

Click here to access/download;Figure;Figure 3.tif

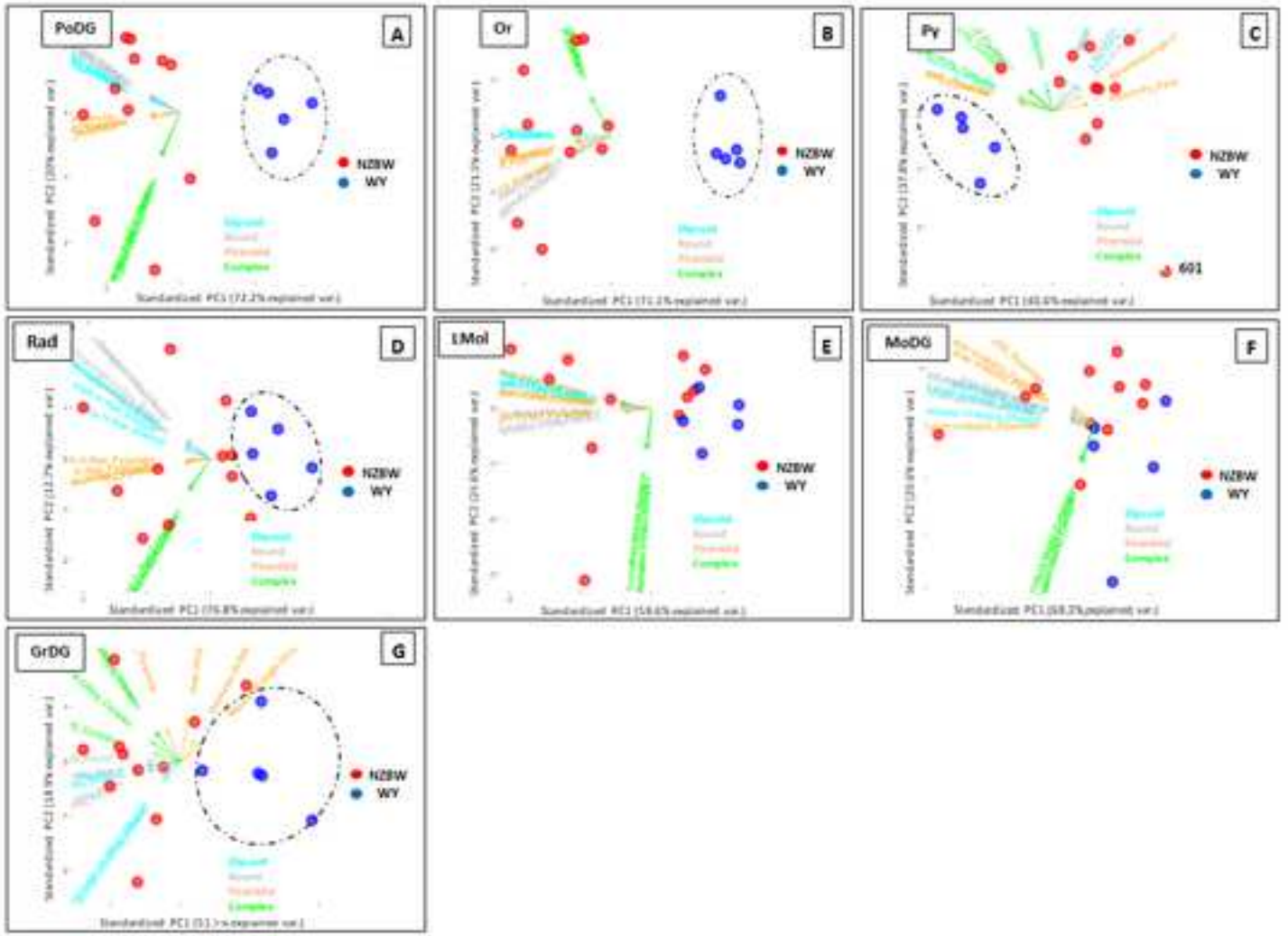

Figure 5

Click here to access/download;Figure;Figure 5.tif

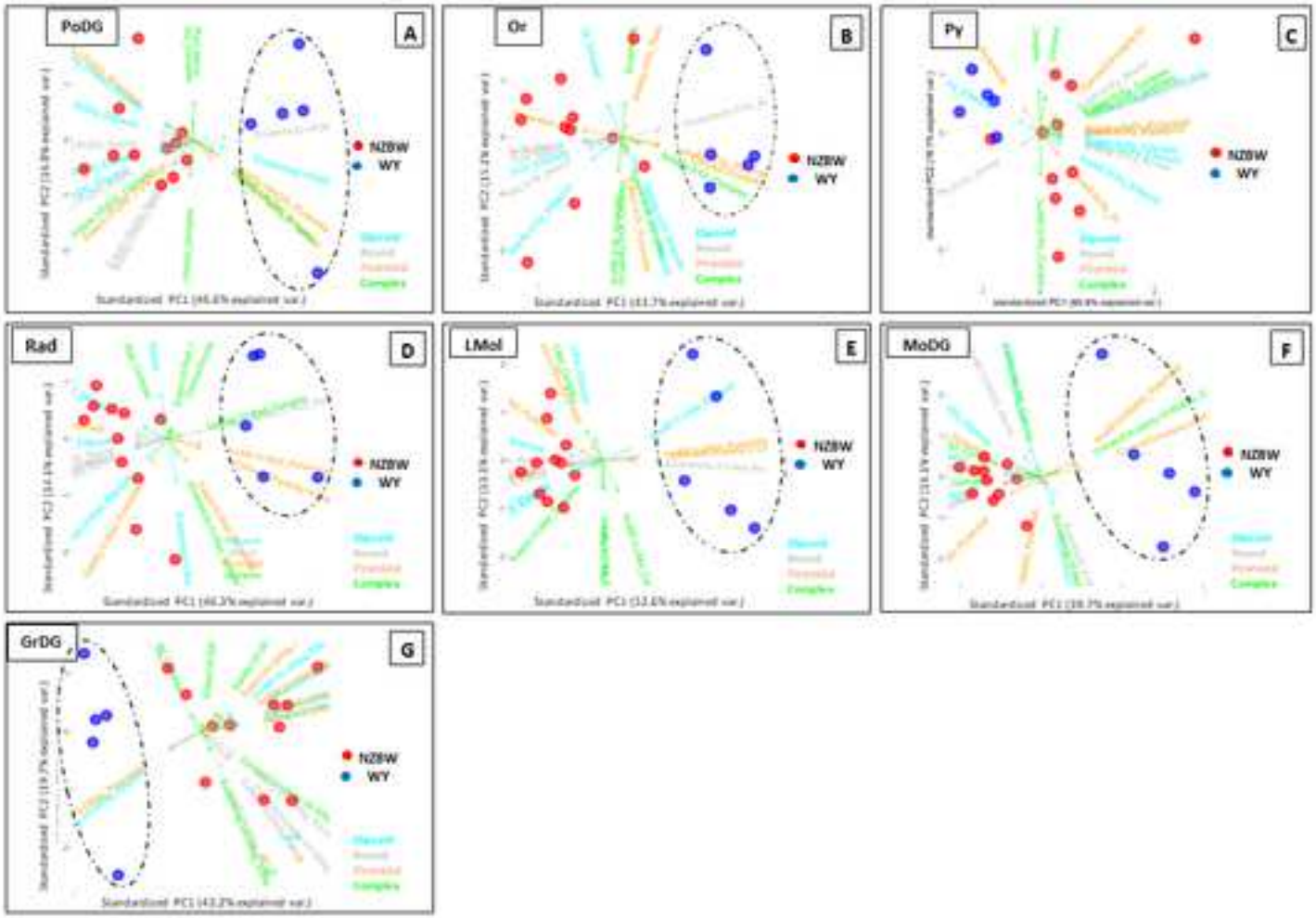

Figure 7

Click here to access/download;Figure;Figure 7.tif

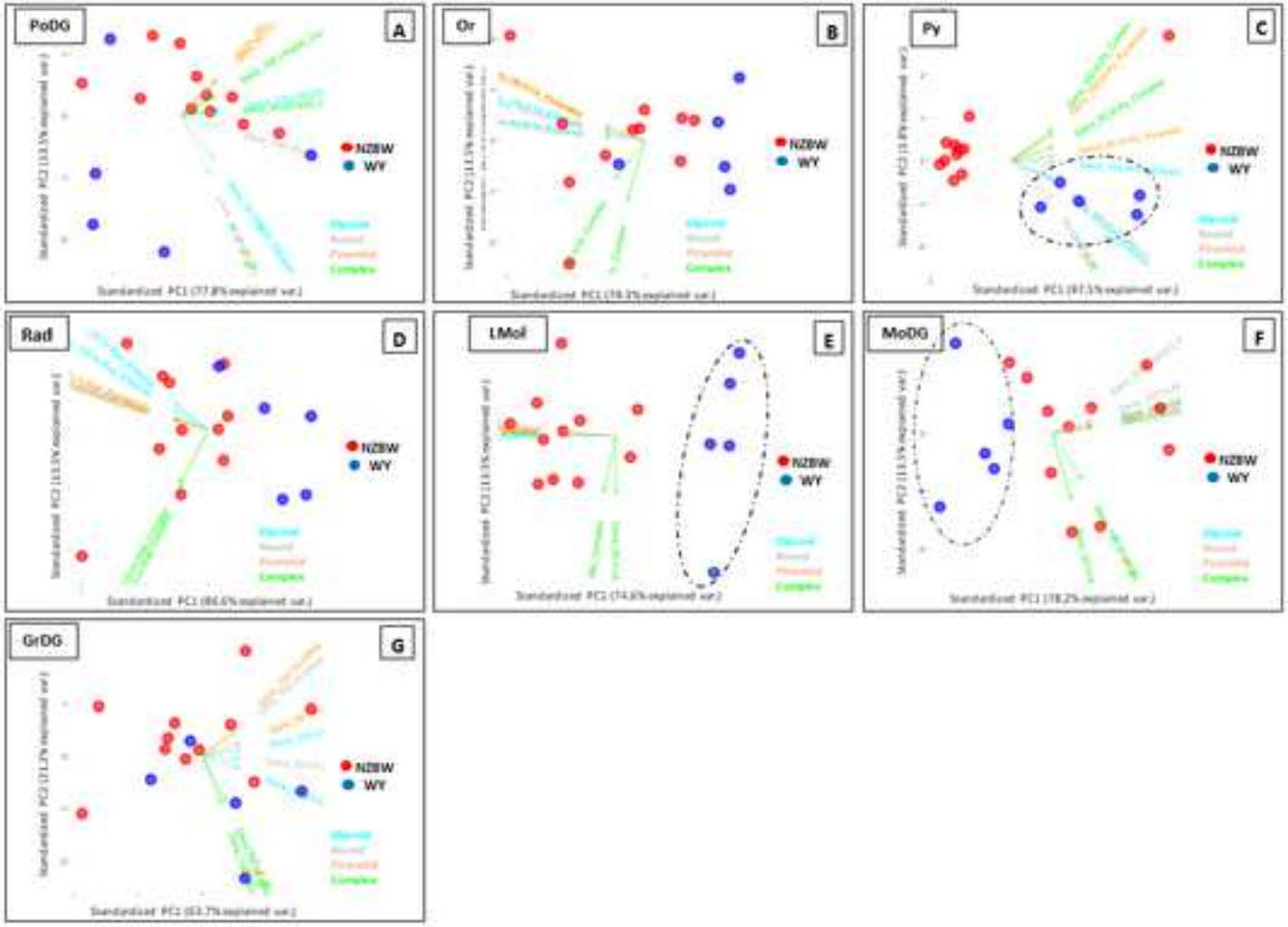

Tables

Table 1

Subregion	cell population Size difference p-value				
	Whole subregion	Round cells	Ellipsoid cells	Pyramidal cells	Complex cells
PoDG	0.0020	0.0030	0.0020	0.0010	0.0410
Or	0.0020	0.0020	0.0010	0.0030	0.0450
Py	0.0080	0.0040	0.0040	0.0020	0.1550
Rad	0.0050	0.0670	0.0020	0.0150	0.0090
LMol	0.0410	0.1530	0.0040	0.0290	0.9530
MoDG	0.0570	0.1530	0.0040	0.0290	0.9530
GrDG	0.0150	0.0010	0.0130	0.1120	0.0200

Table 1: significant p-value combined by subregion and cells shape type for the domain Size with adjustment by multiplicity. The 1% statistically significant p-values are highlighted in bold.

Table 2

Subregion	cell population Regularity difference p-value				
	Whole subregion	Round cells	Ellipsoid cells	Pyramidal cells	Complex cells
PoDG	0.0010	0.0010	0.0010	0.0040	0.3570
Or	0.0010	0.0010	0.0030	0.0010	0.5070
Py	0.0010	0.0140	0.0010	0.0010	0.0840
Rad	0.0010	0.0010	0.0040	0.0010	0.8310
LMol	0.0010	0.0010	0.0010	0.0010	0.2690
MoDG	0.0010	0.0030	0.0030	0.0010	0.0900
GrDG	0.0010	0.0250	0.0510	0.0510	0.2490

Table 2: statistically significant p-value combined by subregion and cells shape type for the Regularity domain with adjustment by multiplicity. The 1% statistically significant p-values are highlighted in bold.

Table 3

Subregion	cell population Density difference p-value				
	Whole subregion	Round cells	Ellipsoid cells	Pyramidal cells	Complex cells
PoDG	0.2330	0.5490	0.4430	0.0550	0.2350
Or	0.0240	0.0200	0.0110	0.0070	0.2210
Py	0.0090	0.0030	0.0040	0.0080	0.0190
Rad	0.0080	0.0030	0.0040	0.0080	0.0080
LMol	0.0090	0.0020	0.0020	0.0020	0.6990
MoDG	0.0090	0.0060	0.0020	0.0020	0.1410
GrDG	0.2330	0.1530	0.0960	0.4110	0.0960

Table 3: statistically significant p-value combined by subregion and cells shape type for the Density domain with adjustment by multiplicity. The 1% statistically significant p-values are highlighted in bold.

Highlights

- Hippocampus is one of the brain structures most sensitive to psychiatric disorders related to neuropsychiatric lupus.
- The NZBW murine model offers an opportunity to bridge the gap between neurological deficits and histological lesions underlying NPSLE.
- Our results show a hypertrophy of the NZB/W F1 hippocampal neurons associated with an increase in perikaryal size.
- By principal component analysis we distinguished healthy Wild Type from NZB/W F1 mice.
- Hippocampal structure in the NZB/W F1 lupus model, suggests the hypothesis that the different subregions could be differentially affected in neuropsychiatric systemic lupus erythematosus disease.